NRL Report 6618

Torque on a Superconducting Toroid in a Uniform Field

B. J. Wilson, E. E. King, and J. R. Miller

Energy Conversion Branch
Electronics Division

December 5, 1967

NAVAL RESEARCH LABORATORY
Washington, D.C.

This document has been approved for public release and sale; its distribution is unlimited.

CONTENTS

Abstract	ii
Problem Status	ii
Authorization	ii
INTRODUCTION	1
THEORETICAL MODEL	2
TORUS	6
TOROID OF ELONGATED CROSS SECTION	10
SPLIT TORUS	11
SPLIT TOROID OF ELONGATED CROSS SECTION	17
A CASE WHERE $\theta_i \neq 0$	18
SUMMARY	20
ACKNOWLEDGMENTS	20
REFERENCES	20

ABSTRACT

The torques on superconducting lead toroids immersed in various uniform fields were measured and calculated as a function of angular position. The calculations, based on ideal superconducting behavior, agree with experiment for the closed torus, if persistent current decrease due to critical surface fields is considered. The recognition of trapped-flux phenomena is needed to explain the measured results for the open torus, when it has been cooled in a nonzero field or when a magnetic transition to superconductivity has been made. The analytical model used magnetic moments for a torus in an axial field and in a perpendicular field, rigorously calculated elsewhere. These methods of obtaining approximations to the moments presented may possibly apply to more general toroidal bodies. The total magnetic moment (and thus the torque) for arbitrary angular position is found by superposition, a result not previously obtained.

PROBLEM STATUS

A final report on one phase of the problem; work on other phases continues.

AUTHORIZATION

NRL Problem E01-01
Project RR 010-04-41-5950.101

Manuscript submitted July 20, 1967.

TORQUE ON A SUPERCONDUCTING TOROID IN A UNIFORM FIELD

INTRODUCTION

The results reported here, along with collateral work by Wright and Peterson (1), cover the principal problems relevant to the torque phenomenon. The underlying magnetic-moment aspects were originally defined by Shoenberg (2) and deLaunay (3) and remained undeveloped for more than a decade. Shoenberg qualitatively analyzed the magnetic behavior for a loop oriented axially coincident with a uniform field; deLaunay solved the magnetic boundary-value problem for the same configuration. The present work, including companion reports (1,4,5) generalizes these earlier attempts to explain magnetization and the consequent torque reaction for the torus and the elongated toroid, both closed (multiply connected) and split (simply connected), at arbitrary angular orientations of the axis in the field. The restricted case of the torus is treated by a predictive or analytical model, corroborated by experiment. The more general elongated toroidal geometry is presented by experimental results, exhibiting qualitatively the characteristics expected from results obtained with the torus.

A departure from the expected torque behavior of a superconducting toroid in a magnetic field led to this investigation of effects concerning the magnetic moment and the torque at arbitrary axial orientations of the toroid. Briefly, two principal, and at first glance almost anomalous, effects were noted from experiments involving toroidal rotation in the field. These were (a) torque limiting effects, and (b) torque hysteresis effects incurred in the first rotation. Initially established values of persistent currents would have produced higher peak torques than those actually experienced if these currents were maintained at the expected levels. If they were not and if they were permanently reduced due to effects encountered during the first rotation, both apparently anomalous effects mentioned above could be explained.

The torque on an ideal, superconducting torus, as it is rotated in a uniform magnetic field, may be calculated by using and extending the aforementioned magnetic-moment notions of Shoenberg and deLaunay. In particular, Shoenberg had anticipated the then unresolved difficulties in deriving the moment for arbitrary orientation in the applied field and had anticipated the presence of such effects as hysteresis and frozen-in fields (6). These effects have been encountered in the experiments reported here and have been resolved by classical methods subject to constraints imposed by superconducting critical conditions.

Based on the experiments and on the adoption of known superconducting phenomena, it is possible to formulate a model which describes torque in terms of Meissner magnetic moments and persistent-current magnetic moments for various initial field and cooling conditions. In developing this model the applied field is resolved into components which remain parallel and perpendicular, respectively, to the torus axis. The magnetic moments generated by either field may then be determined for specific tori from previous evaluations (1,3) and may then be combined by superposition. Evaluation of the parallel-component moments depends upon the results of Shoenberg (2) and deLaunay (3); for the perpendicular-component moment, the results of Wright and Peterson apply (1).

The torque is described by

$$\boldsymbol{T} = \boldsymbol{M} \times \boldsymbol{B},$$

where the total torus moment $\mathbf{M}$ arises from either flux expulsion, persistent current, trapped flux, or a combination of these; $\mathbf{B}$ is the uniform magnetic induction in which the torus is immersed. The details of how these component moments are derived, act in concert, and are constrained by superconducting critical conditions are discussed below and in complementary detail by the separate treatment of Wilson and King (4,5). The basic model is applicable, in principle, to general body shapes, but its use here is restricted to the torus, which serves as a primitive model for electromechanical action, and for which magnetic-moment and field information is available.

THEORETICAL MODEL

This development of the analytical model proceeds directly to the necessary steps for evaluating the working relationships and parameters. Much of the ramifying discussion and derivation is deferred to complementary publications (4,5). Only the definitions and formulas required for the understanding of the remainder of the report are included in this section.

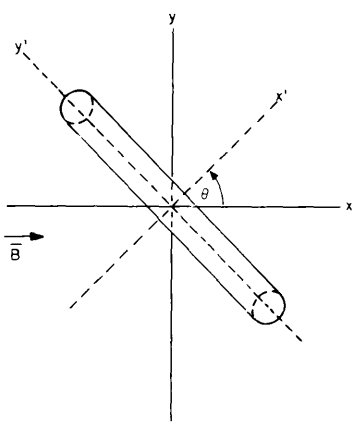

Fig. 1 - Coordinate frames showing the magnetic flux density and the toroid orientation

Figure 1 shows a toroid (which need not have any particular cross-sectional shape) viewed edge on. The externally applied magnetic flux density $\mathbf{B}$ lies along the x axis of the unprimed frame, which is fixed in space. The axis of the toroid lies along the x' axis of the primed frame, which rotates with the toroid about the z' axis. The z and z' axes of the respective coordinate frames are colinear.

The magnetic moment of a nonideal, superconducting toroid (a toroid having imbedded normal regions) which becomes superconducting while oriented so that $\theta = \theta_i$ is

$$\mathbf{M} = \hat{\mathbf{e}}_{x'}\left\{-\left(K_m^{\parallel} + \Delta K_m^{\parallel}\right)B_{x'} - K_c^{\parallel}\left[B_{x'} - B_1(\theta)\right] - \Delta K_c^{\parallel}\left[B_{x'} - B_2(\theta)\right]\right\}$$

$$+ \hat{\mathbf{e}}_{y'}\left\{-\left(K_m^{\perp} + \Delta K_m^{\perp}\right)B_{y'} - \Delta K_c^{\perp}\left[B_{y'} - B_3(\theta)\right]\right\} , \qquad (1)$$

where $\hat{\mathbf{e}}_{x'}$ and $\hat{\mathbf{e}}_{y'}$ are unit vectors along the x' and y' axes, respectively, and where $B_{x'} = \hat{\mathbf{e}}_{x'} \cdot \mathbf{B}$ and $B_{y'} = \hat{\mathbf{e}}_{y'} \cdot \mathbf{B}$.

The K constants, which relate the magnetic moment of a hypothetical, ideal, superconducting toroid (a toroid in which there are no normal regions) to the applied magnetic flux density, are determined by the geometry of the toroid. The subscripts m and c refer to Meissner and to persistent current effects, respectively. $K_m^{\perp}$ and $K_m^{\parallel}$ relate the components of the Meissner magnetic moment, respectively perpendicular and parallel to the axis of the toroid, to the components of the applied magnetic flux density respectively perpendicular to and parallel to the axis of the toroid. $K_c^{\parallel}$ relates the parallel component of the persistent-current magnetic moment to the parallel component of the applied magnetic flux density. One could define a constant $K_c^{\perp}$ in an analogous manner. However, because the projection of the toroid onto a plane parallel to its own axis yields a region which is simply connected, $K_c^{\perp}$ is zero; hence it is not included in the y' component of $\mathbf{M}$ in Eq. (1).

The ΔK's are correction terms arising because the entire volume of the toroid used in the experiments is not superconducting. Actually, they are defined by the geometry of the normal regions imbedded in the toroid in a yet undetermined fashion, but for purposes

of this discussion their determination is limited to evaluation from actual test data. The superscripts and subscripts on the ΔK's have the same meanings as those on the K's. It should be noted that even though $K_c^{\perp}$ is zero, $\Delta K_c^{\perp}$ is not necessarily zero. In effect, $\Delta K_c^{\perp}$ recognizes that the projection of the superconducting portion of the nonideal toroid onto a plane parallel to the toroid's axis and parallel to the axis of rotation is not necessarily a simply connected region.

The parameters $\Delta K_m^{\parallel}$, $\Delta K_m^{\perp}$, $\Delta K_c^{\parallel}$, and $\Delta K_c^{\perp}$ are functions of B, since, in general, as B increases, the imbedded normal regions tend to grow larger. When B is small ($B << B_c$), the ΔK's are assumed to be small in absolute magnitude compared to the corresponding K's (with the exception of $\Delta K_c^{\perp}$), but, when B is near B_c, the imbedded normal regions consume a sizable fraction of the toroidal volume, thus causing the ΔK's to become comparable in absolute magnitude to the corresponding K's (again with the exception of $\Delta K_c^{\perp}$). Because the geometry of the imbedded normal regions depends on the orientation of the toroid with respect to the applied magnetic flux density B, the ΔK's are functions not only of B but also of θ. In addition, it is likely that hysteresis effects are involved in determining the ΔK's. For small values of B, however, the ΔK's are well approximated by constants. It should be remembered that the K's, which relate the magnetic moment of an ideal, superconducting toroid to the applied magnetic flux density, are rigorously constant by virtue of their definition.

The factors $B_1(\theta)$, $B_2(\theta)$, and $B_3(\theta)$ are trapped magnetic flux densities due to the persistent currents. The trapped magnetic flux density $B_1(\theta)$ results from the net persistent current circulating around the opening of the toroid. The trapped magnetic flux density parallel to the axis of the toroid due to the persistent currents circulating around the imbedded normal regions is $B_2(\theta)$. The trapped magnetic flux density perpendicular to the axis of the toroid due to the persistent currents circulating around the imbedded normal regions is $B_3(\theta)$. It is assumed that these trapped magnetic flux densities maintain a fixed orientation with respect to the toroid, while the toroid is rotated relative to the applied, external, magnetic flux density B.

Let θ_i be the angle of toroidal orientation when the toroid becomes superconducting and assume that, after transition to superconductivity, the toroid is rotated in the direction of increasing θ. Assume that, as θ increases, an angle is reached at which the magnetic flux density, at some region of the toroid through which a persistent current is passing, reaches the critical value. The affected region then begins to become normal, thereby tending to reduce the persistent current and its associated trapped magnetic flux density. Thus, as θ increases, the trapped magnetic flux densities monotonically decrease in a way which prevents the magnetic flux densities in the regions through which their associated persistent currents pass from ever exceeding the critical magnetic flux density B_c. Therefore, the trapped magnetic flux densities are written as functions of θ.

The detailed functional dependence of $B_1(\theta)$ is obtained by requiring that the magnetic flux density at any point on the surface of the toroid not exceed the critical value B_c, because the persistent current which sustains $B_1(\theta)$ travels on the surface of the toroid. The magnetic flux density at a point P on the surface of a hypothetical, ideal, superconducting toroid, where P is a variable having two degrees of freedom, is given by

$$B_s(P) = m_1(P)\left(B_1(\theta) - B\cos(\theta)\right) + n_1(P)B\cos(\theta) + p_1(P)B\sin(\theta). \tag{2}$$

The functions $m_1(P)$, $n_1(P)$, and $p_1(P)$ are determined by the geometry of the toroid. One applies the condition that $B_s(P) \leq B_c$ as follows: set $B_1(\theta)$ equal to $B_1(\theta_i)$, the initially trapped magnetic flux density; then attempt, for all $\theta \geq \theta_i$, to find a P such that Eq. (2), with $B_s(P)$ replaced by B_c, is satisfied. The smallest $\theta \geq \theta_i$ for which one can find a P to satisfy the equation is defined to be the critical angle θ_{1c}. This is the angle at which criticality first arises at some point on the toroid's surface, as the toroid is rotated from $\theta = \theta_i$ in the direction of increasing θ. If no θ_{1c} can be found, then criticality never occurs, and $B_1(\theta) = B_1(\theta_i)$ for all θ.

Temporarily treating $B_1(\theta)$ and θ as independent variables in Eq. (2), one may let $P_{max}(\theta, B_1)$ be the point on the surface of the toroid at which $B_s(P)$ is a maximum. Then, for a given θ such that $\theta_{1c} \leqq \theta \leqq \theta_{1min}$, $B_1(\theta)$ is defined to be that B_1 such that this maximum $B_s(P)$ is equal to B_c, where θ_{1min} is the smallest angle at which the $B_1(\theta)$ defined in this way is a minimum. Now that $B_1(\theta)$ has been specified in this manner, P_{max} may be considered to be a function only of θ.

Thus,

$$B_1(\theta) = \begin{cases} B_1(\theta_i), \text{ the initially trapped magnetic flux density}, & \theta_i \leqq \theta \leqq \theta_{1c} \\ \dfrac{B_c}{m_1 P_{max}(\theta)} + \left[1 - \dfrac{n_1 P_{max}(\theta)}{m_1 P_{max}(\theta)}\right] B\cos(\theta) - \dfrac{p_1 P_{max}(\theta)}{m_1 P_{max}(\theta)} B\sin(\theta), & \theta_{1c} \leqq \theta \leqq \theta_{1min} \\ \left\{\dfrac{B_c}{m_1 P_{max}(\theta)} + \left[1 - \dfrac{n_1 P_{max}(\theta)}{m_1 P_{max}(\theta)}\right] B\cos(\theta) - \dfrac{p_1 P_{max}(\theta)}{m_1 P_{max}(\theta)} B\sin(\theta)\right\}_{\theta=\theta_{1min}}, & \theta_{1min} \leqq \theta. \end{cases} \tag{3}$$

A similar method may be used to find $B_2(\theta)$ and $B_3(\theta)$. However, the geometrical structure of the imbedded, normal regions is quite complex, and it is exceedingly difficult to obtain any detailed information about this structure, either by theoretical calculations or by direct measurement. Nevertheless, through the consideration of certain qualitative features of experimental data, and through the application of simplifying assumptions, one may hypothesize the following criticality conditions which $B_2(\theta)$ and $B_3(\theta)$ must satisfy:

$$B_c \geqq \left[B_2(\theta) - B\cos(\theta)\right] m_2 + n_2 B\cos(\theta) \tag{4}$$

$$B_c \geqq \left[B_3(\theta) - B\sin(\theta)\right] m_2 + n_2 B\sin(\theta), \tag{5}$$

where m_2 and n_2 are not to be considered as functions of position. The validity of these inequalities must be judged on the basis of how well the theoretical model derived from them fits the experimental data to be presented later. The definitions of θ_{2c}, θ_{2min}, θ_{3c}, and θ_{3min} are analogous to those of θ_{1c} and θ_{1min}. One finds that

$$\theta_{2c} = \arccos\left[\frac{B_c - m_2 B_2(\theta_i)}{(n_2 - m_2)B}\right], \quad \theta_{2min} = \pi,$$

$$\theta_{3c} = \arcsin\left[\frac{B_c - m_2 B_3(\theta_i)}{(n_2 - m_2)B}\right], \quad \theta_{3min} = \frac{3\pi}{2}.$$

Then,

$$B_2(\theta) = \begin{cases} B_2(\theta_i) = B_i\cos(\theta_i), & \theta_i \leqq \theta \leqq \theta_{2c} \\ \dfrac{B_c}{m_2} + \left(1 - \dfrac{n_2}{m_2}\right) B\cos(\theta), & \theta_{2c} \leqq \theta \leqq \pi \\ \dfrac{B_c}{m_2} - \left(1 - \dfrac{n_2}{m_2}\right) B, & \pi \leqq \theta \end{cases} \tag{6}$$

and

$$B_3(\theta) = \begin{cases} B_3(\theta_i) = -B_i \sin(\theta_i), & \theta_i \leqq \theta \leqq \theta_{3c} \\ \dfrac{B_c}{m_2} + \left(1 - \dfrac{n_2}{m_2}\right) B \sin(\theta), & \theta_{3c} \leqq \theta \leqq \dfrac{3\pi}{2} \\ \dfrac{B_c}{m_2} - \left(1 - \dfrac{n_2}{m_2}\right) B, & \dfrac{3\pi}{2} \leqq \theta . \end{cases} \tag{7}$$

Note that when $B_2(\theta_i) < (B_c/m_2) + [1 - (n_2/m_2)]B$, the angle θ_{2c} does not exist. This means that, regarding the currents sustaining $B_2(\theta)$, criticality never occurs. As a result, $B_2(\theta) = B_2(\theta_i)$ for all θ. In particular, if $B_2(\theta_i) = 0$, then $B_2(\theta) \equiv 0$. This also occurs for $B_3(\theta)$ when $B_3(\theta_i) < (B_c/m_2) + [1 - (n_2/m_2)]B$.

If B_i is the value of B when the toroid becomes superconducting, then $B_1(\theta_i) = B_2(\theta_i) = B_i \cos(\theta_i)$ and $B_3(\theta_i) = -B_i \sin(\theta_i)$. Equations (3), (6), and (7) are not valid if B changes while the toroid is being rotated, although stepwise changes in B (with respect to variations in θ) may sometimes be accommodated by a suitable adjustment of θ_i, $B_1(\theta_i)$, $B_2(\theta_i)$, and $B_3(\theta_i)$.

The torque exerted on the toroid by the applied field is $\boldsymbol{T} = \boldsymbol{M} \times \boldsymbol{B}$, which may be calculated using Eqs. (1), (3), (6), and (7). The $\boldsymbol{T}$ thus determined constitutes the basic theoretical model. The equations comprising the theoretical model are summarized below:

$$\begin{aligned} \boldsymbol{T} = -\hat{e}_z \Big\{ & \left[K_c^{\parallel} B_1(\theta) + \Delta K_c^{\parallel} B_2(\theta)\right] B \sin(\theta) \\ & + \frac{1}{2}\left(K_m^{\perp} - K_m^{\parallel} - K_c^{\parallel} + \Delta K_m^{\perp} - \Delta K_m^{\parallel} - \Delta K_c^{\parallel} + \Delta K_c^{\perp}\right) B^2 \sin(2\theta) - \Delta K_c^{\perp} B_3(\theta)\, B \cos(\theta) \Big\} , \end{aligned} \tag{8}$$

where

$$B_1(\theta) = \begin{cases} B_1(\theta i) = B_i \cos(\theta_i), & \theta_i \leqq \theta \leqq \theta_{1c} \\ \dfrac{B_c}{m_1 P_{\max}(\theta)} + \left[1 - \dfrac{n_1 P_{\max}(\theta)}{m_1 P_{\max}(\theta)}\right] B \cos(\theta) - \dfrac{p_1 P_{\max}(\theta)}{m_1 P_{\max}(\theta)} B \sin(\theta), & \theta_{1c} \leqq \theta \leqq \theta_{1\min} \\ \left\{ \dfrac{B_c}{m_1 P_{\max}(\theta)} + \left[1 - \dfrac{n_1 P_{\max}(\theta)}{m_1 P_{\max}(\theta)}\right] B \cos(\theta) - \dfrac{p_1 P_{\max}(\theta)}{m_1 P_{\max}(\theta)} B \sin(\theta) \right\}_{\theta = \theta_{1\min}}, & \theta_{1\min} \leqq \theta . \end{cases} \tag{3}$$

(θ_{1c} and $\theta_{1\min}$ are obtained by the method described in the text between Eq. (2) and Eq. (3).)

$$B_2(\theta) = \begin{cases} B_2(\theta_i) = B_i \cos(\theta_i), & \theta_i \leqq \theta \leqq \theta_{2c} \\ \dfrac{B_c}{m_2} + \left(1 - \dfrac{n_2}{m_2}\right) B \cos(\theta), & \theta_{2c} \leqq \theta \leqq \pi \\ \dfrac{B_c}{m_2} - \left(1 - \dfrac{n_2}{m_2}\right) B, & \pi \leqq \theta \end{cases} \tag{6}$$

$$\theta_{2c} = \arccos\left[\frac{B_c - m_2 B_i \cos(\theta_i)}{(n_2 - m_2) B}\right]$$

$$B_3(\theta) = \begin{cases} B_3(\theta_i) = -B_i \sin(\theta_i), & \theta_i \leqq \theta \leqq \theta_{3c} \\ \dfrac{B_c}{m_2} + \left(1 - \dfrac{n_2}{m_2}\right) B \sin(\theta), & \theta_{3c} \leqq \theta \leqq \dfrac{3\pi}{2} \\ \dfrac{B_c}{m_2} - \left(1 - \dfrac{n_2}{m_2}\right) B, & \dfrac{3\pi}{2} \leqq \theta \end{cases} \tag{7}$$

$$\left(\theta_{3c} = \arcsin\left[\frac{B_c + m_2 B_i \sin(\theta_i)}{(n_2 - m_2) B}\right]\right)$$

This model is rather general. It applies to toroids of arbitrary cross-sectional shape, to toroids becoming superconducting at arbitrary initial angles θ_i, and to toroids made of materials whose properties differ in various degrees from those of an ideal superconductor. The model is equally valid whether the entry to the superconducting state is via a thermal or a magnetic transition. However, in the case of a magnetic transition, B_i may not be so easily ascertained as in the case of a thermal transition. By setting $K_c^{\parallel}$ and $B_1(\theta)$ equal to zero one may even apply Eq. (8) to the case of a split toroid (a toroid having a thin cross-sectional slice removed).

Nevertheless, there are important limitations on the applicability of the model, due to various approximations used in the derivation; there are also important limitations on the model's usefulness, due to the difficulty involved in calculating certain quantities in the equations. For example, the equations for $B_1(\theta)$, $B_2(\theta)$, and $B_3(\theta)$ may be expected to fail when B is near B_c; the relatively simple notions used in deriving these equations are not true when B assumes values of this magnitude. (It should be recalled that Eqs. (3), (6), and (7) cannot be used if B varies with θ or time, except in certain special cases.) The ΔK's in the equation for T may be approximated by constants only when B is small. A theoretical calculation of the dependence of the ΔK's on B and θ when B is large appears to involve great difficulties. The K's in Eq. (8) and $m_1(P)$, $n_1(P)$, and $p_1(P)$ in Eq. (3) can be readily calculated only for toroids having simple cross-sectional shapes. No simple method has been found for theoretically evaluating the constants m_2 and n_2 appearing in Eqs. (6) and (7).

In the remainder of this report the results predicted by the theoretical model are compared with the results found experimentally in various special cases, chosen to illustrate significant features of the relationship between T and θ.

TORUS

The constants $K_m^{\parallel}$, $K_m^{\perp}$, and $K_c^{\parallel}$, as well as the functions $m_1(P)$, $n_1(P)$, and $p_1(P)$, have been rigorously calculated for a toroid of circular cross section (1,3) and are tabulated in Table 1 (with Fig. 2 explaining the geometrical quantities involved). The quantities $\Delta K_c^{\parallel}$ and $\left(\Delta K_m^{\perp} - \Delta K_m^{\parallel} - \Delta K_c^{\parallel} + \Delta K_c^{\perp}\right)$ are assumed to be small for small B. (It will be shown in the part of this report dealing with the split torus that this assumption is reasonably well justified.) So, an approximation to Eq. (8), valid for small B, is

$$T = -e_z\left[K_c^{\parallel} B_1(\theta) B \sin(\theta) + \frac{1}{2}\left(K_m^{\perp} - K_m^{\parallel} - K_c^{\parallel}\right) B^2 \sin(2\theta)\right], \tag{9}$$

where, for simplicity, θ_i has been taken equal to zero (thus making $B_3(\theta)$ identically zero). It should be remembered that Eq. (3), which furnishes the $B_1(\theta)$ used in Eq. (9), is itself an approximation, valid only for values of B which are not too large.

Table 1
Calculated Values of the Moment Constants for a Toroid Having a Circular Cross Section

$s = R/r$ *	$K_m^{\parallel}/V$ †	$K_m^{\perp}/V$ †	$K_c^{\parallel}/V$ †	$m_1(P)$ ‡		$n_1(P)$ ‡		$p_1(P)$ ‡	α At Which $P_1(P)$ is Evaluated ‡
				$\alpha = 0$	$\alpha = 180°$	$\alpha = 0$	$\alpha = 180°$		
1.0	0.163	0.10902	—	—	—	—	—	—	—
1.1	—	0.10809	—	—	—	—	—	—	—
1.2	0.16501	0.10818	0.00893	4.743	0.01562	4.743	1.808	1.599	90°
1.4	0.16549	0.10881	0.02322	3.569	0.04870	3.569	1.829	1.635	91°
1.6	0.16521	0.10966	0.03989	3.094	0.06998	3.092	1.845	1.670	92°
1.8	0.16474	—	0.05820	2.837	0.10110	2.830	1.857	—	—
2.0	0.16424	0.11138	0.07780	2.679	0.13330	2.666	1.867	1.736	94°
3.0	0.16234	0.11437	0.19161	2.403	0.29813	2.324	1.900	1.843	96°
4.0	0.16130	—	0.32862	2.384	0.45937	2.209	1.919	—	—
5.0	0.16071	0.11691	0.48715	2.436	0.61434	2.153	1.931	1.927	95°
6.0	0.16034	—	0.66628	2.517	0.76341	2.120	1.940	—	—
7.0	0.16008	0.11790	0.86533	2.611	0.90736	2.098	1.947	1.958	94°
8.0	0.15990	—	1.08374	2.712	1.0469	2.083	1.952	—	—
9.0	0.15978	—	1.3164	2.818	1.1827	2.072	1.957	—	—
10.0	0.15968	0.11854	1.5767	2.925	1.3152	2.063	1.960	1.976	93°
	0.15915	0.11936	—	—	—	—	—	—	—

*See Fig. 2 for the definitions of r and R.
†The K constants are given in Gaussian units, and V is the volume of the torus in cm^3 (i.e., the units of K/V are dyne-cm/G^2-cm^3). $K_m^{\parallel}/V$ is translated from Ref. 3, $K_m^{\perp}/V$ from Ref. 1, and $K_c^{\parallel}/V$ from Ref. 2.
‡The point P at which m_1, n_1, and p_1 are evaluated is chosen to lie in the section plane AA shown in Fig. 2. See Fig. 2 for the definition of α. $m_1(P)$, $n_1(P)$, and $p_1(P)$ are obtained from Refs. 1 and 3.

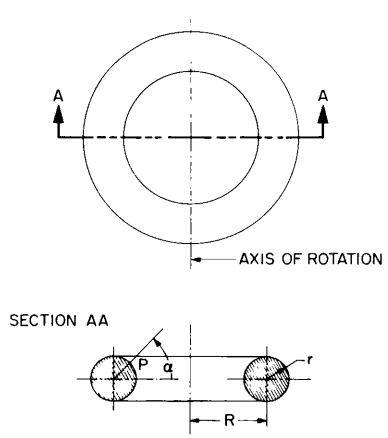

Fig. 2 - Geometry of the torus

The experiments against which Eq. (9) was tested were performed with a well-annealed torus constructed of lead having 0.9999 purity. The dimensions of the torus are R = 0.875 in. and r = 0.125 in. (Fig. 2).

Figure 3 shows both the empirical and the theoretically predicted torques for an experiment in which the externally applied magnetic flux density B is initially 200 G while the torus is being cooled into the superconducting state with $\theta = \theta_i = 0$, is then reduced to 100 G, and is maintained at 100 G while θ is increased from 0 to 4π. The portion of the graph for which $2\pi \leqq \theta \leqq 4\pi$ is superposed on the portion for which $0 \leqq \theta \leqq 2\pi$, so that the hysteresis effects due to the occurrence of criticality may be more clearly seen. The agreement between the measured torques and the theoretically predicted torques is seen to be fairly good. The existing discrepancy, especially in the ranges $\pi \leqq \theta \leqq 2\pi$ and $3\pi \leqq \theta \leqq 4\pi$, is probably due to the experimental error involved in measuring B, B_i, and B_c, because the torque predicted by Eq. (9) is fairly sensitive to variations in these quantities. For example, if the B and $B_1(\theta)$ used in the theoretical calculations are each decreased by only 10 G from their measured values of 100 G and 200 G respectively, and if the B_c used in these calculations is increased by 50 G from its "handbook value" of 540 G, then the theoretical and empirical curves agree very well (5).

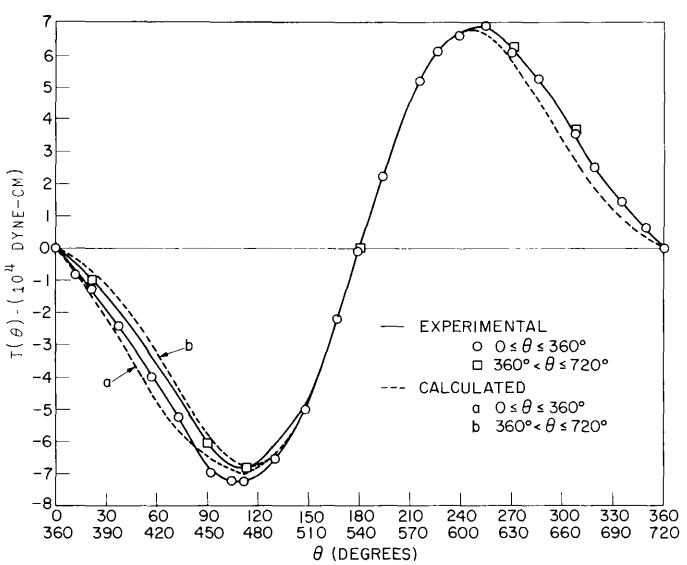

Fig. 3 - Torque for the torus cooled with B = 200 G and θ = 0, and rotated with B = 100 G

Figure 4 shows the predicted and measured torques for a continuation of this experiment. The torus is kept in the superconducting state and remains at the angle $\theta = 0$ (formerly denoted by $\theta = 4\pi$) while B is increased from 100 G to 200 G. Then the torus is again rotated in the direction of increasing θ, through a total angular displacement of 4π radians, while B is held constant at 200 G. One would intuitively expect that this higher value of B would make the effects of criticality more prominent than they were in that part of the experiment portrayed by Fig. 3. This expectation is confirmed by an examination of the experimental curves of Fig. 4. The difference between $T(\theta)$ and $T(\theta + 2\pi)$ in the range $0 \leqq \theta \leqq \pi$ is much greater with the 200-G applied magnetic flux density (Fig. 4) than with the 100-G applied magnetic flux density (Fig. 3). The theoretical curves of Fig. 4 are again calculated using Table 1 and Eqs. (9) and (3), but in this case B_i is set equal to the $B_1(\theta_{1\min})$ found for that part of the experiment for which B = 100 G ($\theta_i = 0$, as before). The predicted and measured curves agree reasonably well, but the agreement can be improved by again changing the B and the B_c used in the calculations from 200 G and 540 G, respectively, to 190 G and 590 G, respectively (5).

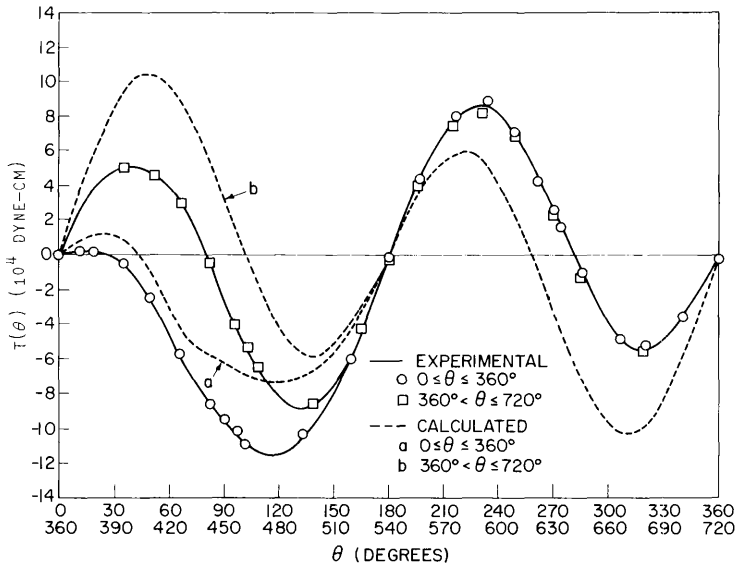

Fig. 4 - Continuation of Fig. 3. At $\theta = 0$, B is raised to 200 G; the torus is then rotated with B = 200 G.

It should be noted that when B is 100 G (Fig. 3) the torque exhibits a predominantly $\sin(\theta)$ angular dependence, and when B is increased to 200 G (Fig. 4) the torque exhibits a predominantly $\sin(2\theta)$ dependence for $\theta \geqq \pi$. In terms of Eqs. (3) and (9) this alteration in the form of the angular dependence may be explained by an increase in B in Eq. (3) causing a decrease in $B_1(\theta)$, and a decrease in $B_1(\theta)$ causing the $\sin(\theta)$ term in Eq. (9) to become smaller relative to the $\sin(2\theta)$ term. In addition, the $\sin(2\theta)$ term in Eq. (9) contains B^2, while the $\sin(\theta)$ term contains B. The fact that Eqs. (3) and (9) predict the fundamental change in the character of the angular dependence of the torque when B is increased from 100 G to 200 G attests strongly to the overall correctness of these equations for values of B which are not too large.

Figure 5 shows additional experimental data obtained in an extension of this experiment. Immediately after the completion of the portion of the experiment illustrated by Fig. 4, $\theta = 0$ (denoted in Fig. 4 by $\theta = 4\pi$) and B = 200 G. The magnetic induction is then increased to 300 G and held at this value while the torus is rotated through 4π radians. Finally, while the orientation of the torus is maintained at $\theta = 0$ (formerly denoted by $\theta = 4\pi$), B is increased to 400 G. B is held at this value while the torus is once more rotated through 4π radians. The theoretical predictions of Eq. (9) are not shown in Fig. 5, because, even without plotting them, one can readily see from Eq. (9) that the torques which it predicts differ substantially from the torques actually observed. One can see from Fig. 4 that the $\sin(\theta)$ term is almost negligible compared to the $\sin(2\theta)$ term, even with B as low as 200 G. Therefore, one is certainly safe in ignoring the $\sin(\theta)$ term when using Eq. (9) to make estimates of the predicted peak-to-peak amplitude of $T(\theta)$ for B = 300 G and for B = 400 G. Equation (9) indicates that the peak-to-peak amplitude of the curve $T(\theta)$ for B = 300 G should be approximately 9/4 of the peak-to-peak amplitude of the curve $T(\theta)$ for B = 200 G. However, comparing the experimental curves in Figs. 4 and 5 shows that, in reality, the peak-to-peak amplitude of the curve $T(\theta)$ for 300 G is approximately 3/4 of the peak-to-peak amplitude of the curve $T(\theta)$ for B = 300 G. Similarly, it can be seen that Eq. (9) predicts a peak-to-peak amplitude of the curve $T(\theta)$ for B = 400 G which is approximately 20 times too large.

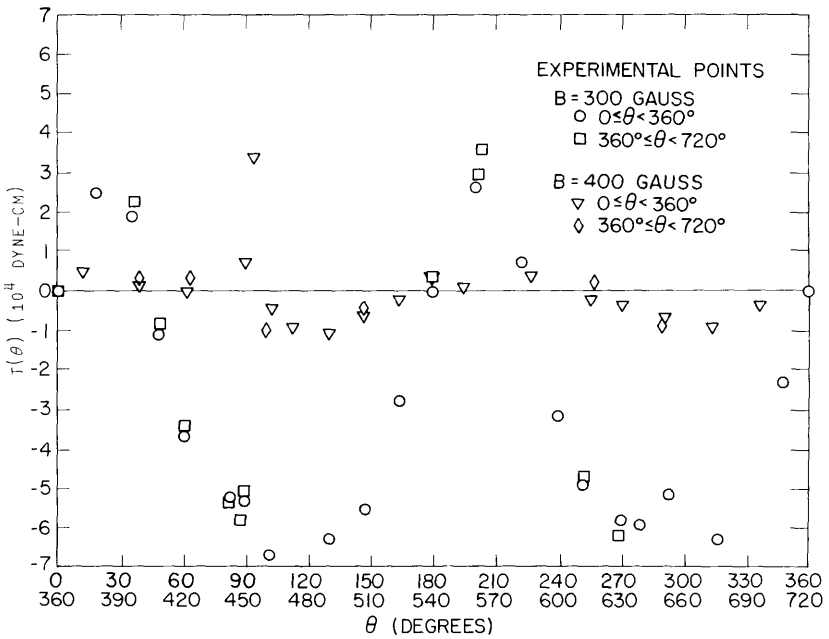

Fig. 5 - Continuation of Fig. 4. At $\theta = 0$, B is raised to 300 G; the torus is then rotated with $B = 300$ G and with $B = 400$ G.

The failure of Eq. (9) at high values of B is probably due primarily to failures in the approximations used in deriving Eq. (9) from Eq. (8). One cannot neglect $\Delta K_c^{\parallel}$ with respect to $K_c^{\parallel}$ or $(\Delta K_m^{\perp} - \Delta K_m^{\parallel} - \Delta K_c^{\parallel} + \Delta K_c^{\perp})$ with respect to $(K_m^{\perp} - K_m^{\parallel} - K_c^{\parallel})$ when B is near B_c. Of course, Eqs. (3), (6), and (7) are unreliable for large B, but the terms in Eq. (8) which contain $B_1(\theta)$ and $B_2(\theta)$ are negligible for large B. (Note the indiscernability of hysteresis effects in the experimental curves shown in Fig. 5.)

By inspecting the experimental curve $T(\theta)$ for $B = 300$ G in Fig. 5, one can see that

$$\int_{2\pi}^{4\pi} \tau(\theta)\, d\theta$$

is substantially greater than zero. Thus, if the experimental curve $T(\theta)$ for $B = 300$ G is to be believed, a net amount of energy is put into the system during the rotation of the torus from $\theta = 2\pi$ to $\theta = 4\pi$. However, no sink for this energy is apparent. Therefore, if the conservation-of-energy law is not to be violated, one is forced to the conclusion that some systematic experimental error has caused the line $T = 0$ to shift from its correct position. A similar, though smaller, shift seems to have occurred in the data corresponding to $B = 400$ G.

TOROID OF ELONGATED CROSS SECTION

Figure 6 shows the geometry of the toroid of elongated cross section used in these experiments. The toroid is made of well-annealed lead having 0.9999 purity.

Equations (3) and (9) apply in this case, provided B is small enough. However, Table 1, which applies only to toroids of circular cross section, cannot be used. The

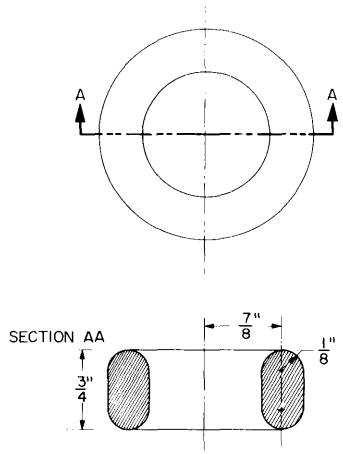

Fig. 6 - Geometry of the toroid of elongated cross section

problem of rigorously computing $K_m^{\perp}$, $K_m^{\parallel}$, $K_c^{\parallel}$, $m_1(P)$, $n_1(P)$, and $p_1(P)$ for a toroid having a geometry like that shown in Fig. 6 has never been solved, and no one has yet found any practical method for theoretically approximating these quantities accurately.

Figure 7 shows the experimental results when the toroid of Fig. 6 is cooled into the superconducting state with the applied magnetic flux density B equal to 200 G and with the orientation angle θ equal to zero. Then B is reduced to 100 G and maintained at this value while the toroid is rotated through 4π radians. The small difference between $T(\theta)$ and $T(\theta + 2\pi)$ in the range $0 \leqq \theta \leqq \pi$ indicates that the effects of criticality are essentially negligible in this case. Thus, to a good approximation, $B_1(\theta)$ may be taken to equal $B_1(0) = B_i$ for all θ. Then the coefficients of $\sin(\theta)$ and $\sin(2\theta)$ in Eq. (9) are independent of θ. Experimental values may be assigned to these coefficients by least-square curve fitting, using the experimental data points for $0 \leqq \theta \leqq 2\pi$ shown in Fig. 7. It is

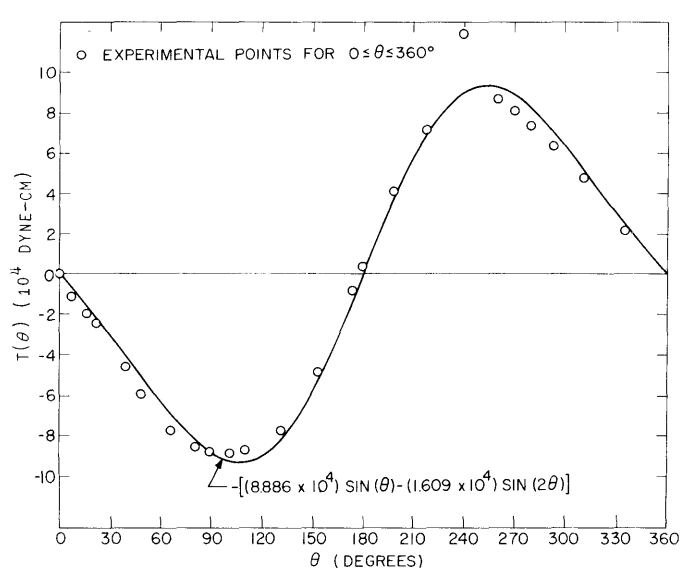

Fig. 7 - Torque of the toroid of elongated cross section cooled with B = 200 G and θ = 0, and rotated with B = 100 G

found that $K_c^{\parallel} B_1(0) B = 8.886 \times 10^4$ dyne-cm and that $1/2\ (K_m^{\perp} - K_m^{\parallel} - K_c^{\parallel}) B^2 = -1.609 \times 10^4$ dyne-cm. Thus, since $B = 100$ G and $B_1(0) = 200$ G, it follows that

$$K_c^{\parallel} = 4.443 \text{ dyne-cm/G}^2 \text{ and } K_m^{\perp} - K_m^{\parallel} = 1.225 \text{ dyne-cm/G}^2.$$

Although, as previously stated, no relatively simple method for theoretically approximating $K_m^{\perp}$ and $K_m^{\parallel}$ accurately has been developed, one can obtain rough theoretical estimates of these quantities by using an ellipse of appropriate size and shape to approximate the toroid's actual cross section. The hypothetical toroid of elliptical cross section used in this estimation is illustrated in Fig. 8. It has been determined that if $b << R$ and $c << R$, then, to a good approximation, the Meissner constants for this type of toroid are given by

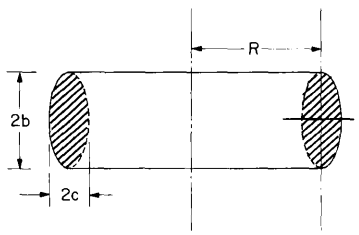

Fig. 8 - Geometry of a hypothetical toroid of elliptical cross section to approximate the cross section of the toroid shown in Fig. 6

$$\frac{K_m^{\perp}}{V} = \frac{1}{4\pi}\left(1 + \frac{b}{2c}\right) \text{ and } \frac{K_m^{\parallel}}{V} = \frac{1}{4\pi}\left(1 + \frac{c}{b}\right),$$

where V is the volume of the toroid and $K_m^{\perp}/V$ and $K_m^{\parallel}/V$ are expressed in units of dyne-cm/G^2 cm^3 (1). Then

$$K_m^{\perp} - K_m^{\parallel} = \frac{\pi R}{4}\,(b^2 - 2c^2),$$

where $K_m^{\perp}$ and $K_m^{\parallel}$ are in units of dyne-cm/G^2 and R, b, and c are in units of centimeters. One is faced with the problem of choosing R, b, and c so that this equation, which approximates $(K_m^{\perp} - K_m^{\parallel})$ for the hypothetical toroid, will apply with acceptable accuracy to the actual toroid of elongated cross section.

One simple approach is to choose R equal to the corresponding dimension of the toroid of elongated cross section and to choose the width and length of the elliptical cross section to be respectively equal to the width and length of the elongated cross section of the actual toroid; that is, one would set $R = 7/8$ in. = 2.223 cm, $b = 3/8$ in. = 0.9525 cm, and $c = 1/8$ in. = 0.3175 cm. This choice yields 1.232 dyne-cm/G^2 as the theoretically predicted value of $(K_m^{\perp} - K_m^{\parallel})$, providing good agreement with the experimentally obtained value of 1.225 dyne-cm/G^2.

One may estimate $K_c^{\parallel}$ fairly easily. The projection of the toroid of elongated cross section (Fig. 6) onto a plane perpendicular to its axis is identical to the corresponding projection of the torus described earlier (Fig. 2 with $R = 7/8$ in. and $r = 1/8$ in.). Therefore, the $K_c^{\parallel}$ for the toroid of elongated cross section should be roughly the same as the $K_c^{\parallel}$ for the torus. Using Table 1, one finds that, for the torus, $K_c^{\parallel} = 3.827$ dyne-cm/G^2. This value is indeed reasonably close to 4.443 dyne-cm/G^2, the experimentally determined value of $K_c^{\parallel}$ for the hypothetical toroid.

Figure 9 shows the results of a continuation of the experiment to which Fig. 8 pertains. While the toroid is held so that $\theta = 0$ (denoted by $\theta = 4\pi$ in Fig. 8) B is increased from 100 G to 200 G. Then the toroid is rotated through 8π radians while B is maintained at 200 G. It is evident from a comparison of Figs. 7 and 9 that the effects of criticality are much more severe when the toroid is rotated with $B = 200$ G than they are when the toroid is rotated with $B = 100$ G. Thus, $B_1(\theta)$ can no longer be taken equal to $B_1(0)$ for all θ, as it was when the rotation of the toroid was carried out with $B = 100$ G. Instead, one must use Eq. (3) to theoretically determine $B_1(\theta)$. However, due to the toroid's relatively complicated cross section, there is no reasonably simple theoretical method for determining the functions $m_1(P)$, $n_1(P)$, and $p_1(P)$ appearing in this equation. Therefore, no attempt is made to quantitatively relate the predictions of Eqs. (3) and (9) to the $T(\theta)$ obtained experimentally.

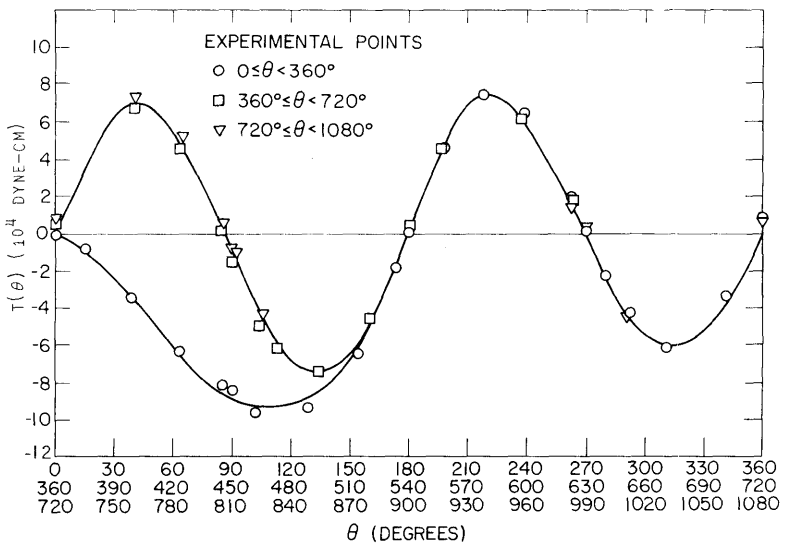

Fig. 9 - Continuation of Fig. 7. At $\theta = 0$, B is raised to 200 G; the toroid is then rotated with $B = 200$ G.

SPLIT TORUS

Figure 10 shows the geometry of the split torus used in the experiment. The split torus is made of well-annealed lead having 0.9999 purity.

For the split torus, which can have no net current around its central opening, $B_1(\theta) \equiv 0$, and $K_c^{\parallel} = 0$. The constants $K_m^{\perp}$ and $K_m^{\parallel}$ are given, to a good approximation, by the values in Table 1, because the cross-sectional slice which has been removed is small.

Let $\Delta X = \Delta K_m^{\perp} + \Delta K_c^{\perp} - \Delta K_m^{\parallel}$. Then Eq. (8) becomes

$$\boldsymbol{T} = -\hat{e}_z \left[\Delta K_c^{\parallel} B B_2(\theta) \sin(\theta) + \frac{1}{2} \left(K_m^{\perp} - K_m^{\parallel} - \Delta K_c^{\parallel} + \Delta X \right) B^2 \sin(2\theta) \right], \tag{10}$$

where, as before, $B_2(\theta)$ is given by Eq. (6), provided B is small enough.

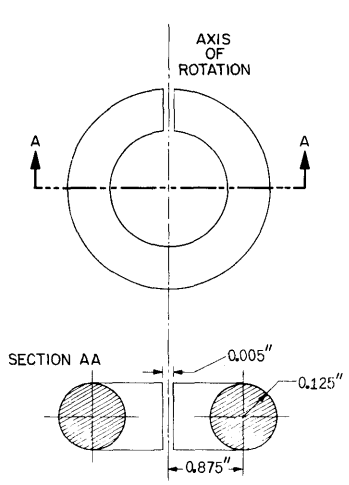

Fig. 10 - Geometry of the split torus

If the split torus becomes superconducting with $B = 0$, then $B_2(\theta)$ will be 0 for all θ, and Eq. (10) predicts that T will exhibit a pure $\sin(2\theta)$ dependence upon θ. Figure 11, which presents the results of an experiment in which the split torus is cooled below the superconducting transition temperature while B is maintained at 0 G, confirms this prediction. However, the theoretically predicted amplitude of $T(\theta)$ is significantly greater than the amplitude actually measured (compare the theoretical and experimental curves in Fig. 11). The most likely cause of this disagreement is a systematic error in the measurement of B, because B appears to the second power in the $\sin(2\theta)$ term of Eq. (10). If the B used in Eq. (10) is decreased by 10% from its measured value, then, the theoretical curve $T(\theta)$ agrees closely with the experimental curve $T(\theta)$ (5).

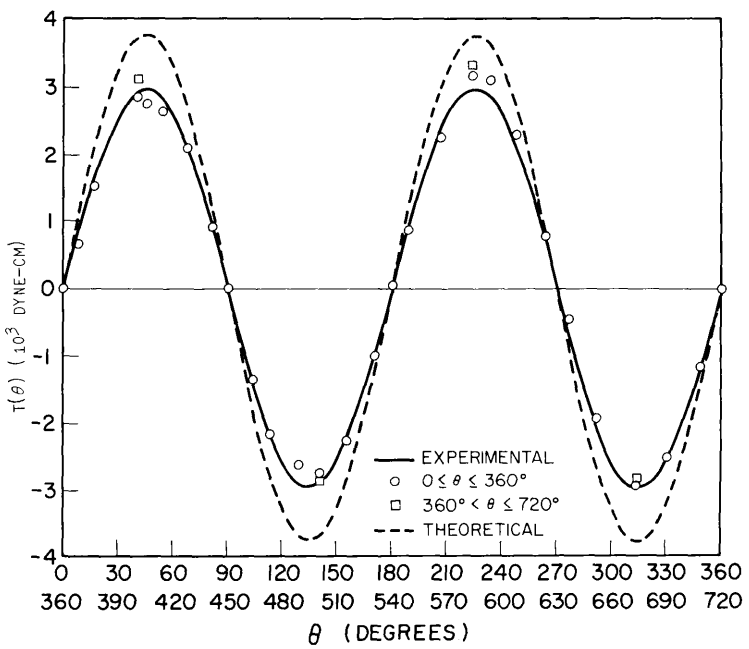

Fig. 11 - Torque for the split torus cooled with $B = 0$ and $\theta = 0$, and rotated with $B = 200$ G

The results of another experiment in which the split torus becomes superconducting with $B = 0$ are shown in Fig. 12. After cooling, B is increased to 100 G, and the split torus is rotated through 2π radians with B held at 100 G. Then B is successively increased to 200 G, 300 G, 400 G, and 500 G, and the split torus is rotated through 2π radians for each value of B.

From this figure one can see qualitatively the effects of criticality on $T(\theta)$ at relatively high values of B. No analytical examination of the experimental data represented by these curves was attempted.

As in Fig. 5, some systematic experimental error seems to have shifted the zero reference of $T(\theta)$ in Fig. 12 from its proper position. The shift appears to be different for each of the curves corresponding to a different value of B.

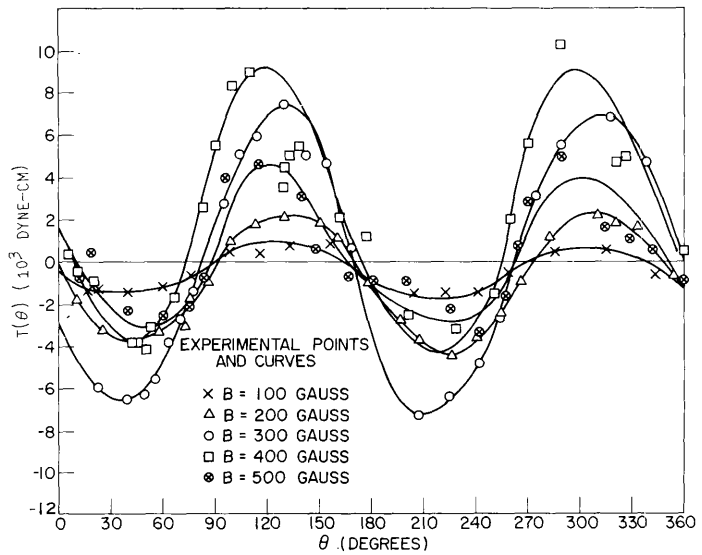

Fig. 12 - Torque for the split torus cooled with $B = 0$ and $\theta = 0$, then successively rotated through 360° with B = 100 G, 200 G, 300 G, and 500 G

If B is not equal to zero when the split torus becomes superconducting, then $B_2(\theta)$ is not identically zero; therefore, the $\sin(\theta)$ term in Eq. (10) may not be omitted. Substituting Eq. (6) with $\theta_i = 0$ into Eq. (10), one obtains

$$\boldsymbol{T} = \begin{cases} -\hat{e}_z \left[C_1 \sin(\theta) + C_2 \sin(2\theta)\right], & 0 \leqq \theta \leqq \theta_{2c} \\ -\hat{e}_z \left[C_3 \sin(\theta) + C_4 \sin(2\theta)\right], & \theta_{2c} \leqq \theta \leqq \pi, \\ -\hat{e}_z \left[C_5 \sin(\theta) + C_6 \sin(2\theta)\right], & \pi \leqq \theta \end{cases} \tag{11}$$

where

$$C_1 = \Delta K_c^{\parallel} B B_i, \quad C_2 = \frac{1}{2}\left(K_m^{\perp} - K_m^{\parallel} - \Delta K_c^{\parallel} + \Delta X\right) B^2, \quad C_3 = \frac{\Delta K_c^{\parallel} B_c B}{m_2},$$

$$C_4 = \frac{1}{2}\left(K_m^{\perp} - K_m^{\parallel} - \frac{n_2}{m_2}\Delta K_c^{\parallel} + \Delta X\right) B^2, \quad C_5 = \left[\frac{B_c B}{m_2} - \left(1 - \frac{n_2}{m_2}\right) B^2\right] \Delta K_c^{\parallel},$$

$$C_6 = \frac{1}{2}\left(K_m^{\perp} - K_m^{\parallel} - \Delta K_c^{\parallel} + \Delta X\right) B^2,$$

and

$$\theta_{2c} = \arccos\left[\frac{B_c - m_2 B_i}{(n_2 - m_2) B}\right].$$

However; no one has yet derived a theoretical calculation that will give reasonably accurate values for $\Delta K_c^{\parallel}$, ΔX, m_2, and n_2. Thus, the six C's and θ_{2c} cannot be determined theoretically. The only check on the theoretical model under these circumstances is to see if Eq. (11) has a form consistent with the experimental data, that is, to see if the

constants $C_1, \ldots, C_6$ and θ_{2c} can be found such that the theoretical curve $T(\theta)$ generated by Eq. (11) is a good fit to the empirical curve. When one has obtained $C_1, \ldots, C_6$ and θ_{2c}, one can solve for $\Delta K_c^{\parallel}$, ΔX, m_2, and n_2. Note that only four of the constants $C_1, \ldots, C_6$ and θ_{2c} are independent, because interrelations among these seven constants are provided by the equations: $C_2 = C_6$; $2C_2 + C_3 = 2C_4 + C_5$; and $\theta_{2c} = \arccos[(C_3 - C_1)/2(C_2 - C_4)]$. One finds that

$$\Delta K_c^{\parallel} = \frac{C_1}{B B_i} \quad , \quad \Delta X = \frac{2C_2}{B^2} + K_m^{\parallel} - K_m^{\perp} + \Delta K_c^{\parallel}$$

($K_m^{\parallel}$ and $K_m^{\perp}$ are found from Table 1),

$$m_2 = \frac{B_c}{B_i} \frac{C_1}{C_3} ,$$

and

$$n_2 = m_2 + \frac{2B_c}{B} \frac{C_2 - C_4}{C_3} .$$

Figure 13 shows the experimental results when the split torus becomes superconducting at B = 200 G with $\theta_i = 0$ and was then rotated through 4π radians while B was maintained at 200 G. Applying least-square curve fitting to the portion of the curve between $\theta = 0$ and $\theta = 2\pi$, one finds that the constants C_1 = 5295 dyne-cm, C_2 = - 3102 dyne-cm, C_3 = 5130 dyne-cm, C_4 = -3013 dyne-cm, C_5 = 4953 dyne-cm, C_6 = - 3102 dyne-cm, and θ_{2c} = 21.21° give a reasonably good fit to the experimental data and simultaneously satisfy the three equations furnishing interrelations among $C_1, \ldots, C_6$, and θ_{2c}. Using these constants one calculates that $\Delta K_c^{\parallel}$ = 0.1324 dyne-cm/G^2, ΔX = 0.1638 dyne-cm/G^2, m_2 = 2.787, and n_2 = 2.694. Note that the values obtained for $\Delta K_c^{\parallel}$ and ΔX support the assumption used in deriving Eq. (9).

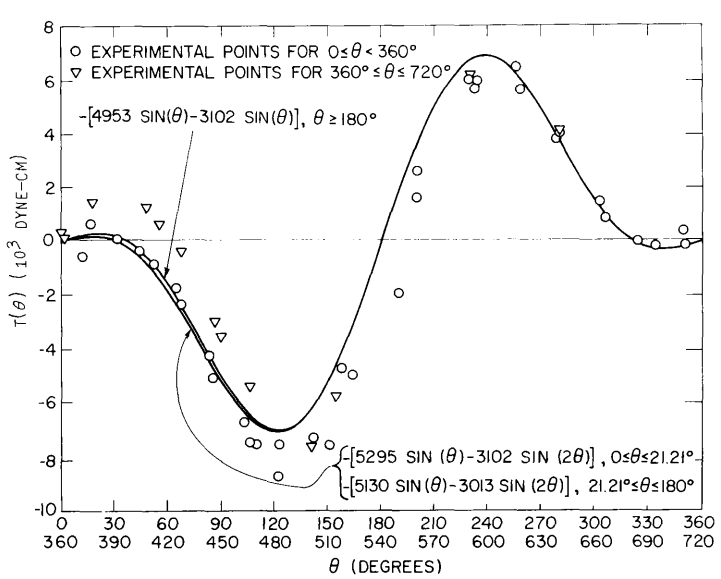

Fig. 13 - Torque for the split torus cooled with B = 200 G and θ = 0, and rotated with B = 200 G

Figure 14 illustrates the experimental outcome when the split torus becomes superconducting by reducing B from 1000 G to 200 G with $\theta_i = 0$ while being maintained at the liquid-helium temperature. It is then rotated through 4π radians while B is maintained at 200 G. To a first approximation the only difference between this experiment and the preceding experiment is in the value of B_i. Because the split torus becomes superconducting through a magnetic transition, it is not obvious what B_i should be in this case. However, Eq. (11) is still applicable, with $C_1, \ldots, C_6$, and θ_{2c} defined as before. Then, subject to the constraints $C_2 = C_6$, $2C_2 + C_3 = 2C_4 + C_5$, and $\theta_{2c} = \arccos[(C_3 - C_1)/2(C_2 - C_4)]$, the least-square fit to the experimental T-versus-θ data displayed in Fig. 9 is given by $C_1 = 6625$ dyne-cm, $C_2 = -3043$ dyne-cm, $C_3 = 5566$ dyne-cm, $C_4 = -2346$ dyne-cm, $C_5 = 4172$ dyne-cm, $C_6 = -3043$ dyne-cm, and $\theta_{2c} = 40.57°$. Assuming that m_2 is the same as in the previous experiment (call it $m_{2\mathrm{prev}}$) one calculates

$$B_i = \frac{B_c}{m_{2\mathrm{prev}}} \frac{C_1}{C_3} = 230.6 \text{ G}.$$

The split torus is in the intermediate state when $B_c/n_1(P_0) < |\mathbf{B}| < B_c$, where P_0 is a point in the section-plane AA shown in Fig. 2 and having $\alpha = 0$. Thus, for the split torus used in this experiment, Table 1 indicates that the approximate B at which a transition between the pure superconducting state and the intermediate state should occur is 540 G/2.098 = 257 G. The closeness of this value to the value of B_i suggests that, as the absolute magnitude of B is lowered, flux trapping takes place when B is equal to the value at which a transition between the intermediate and the pure superconducting states is predicted. Certain researches conducted by others tend to support this view (7,8).

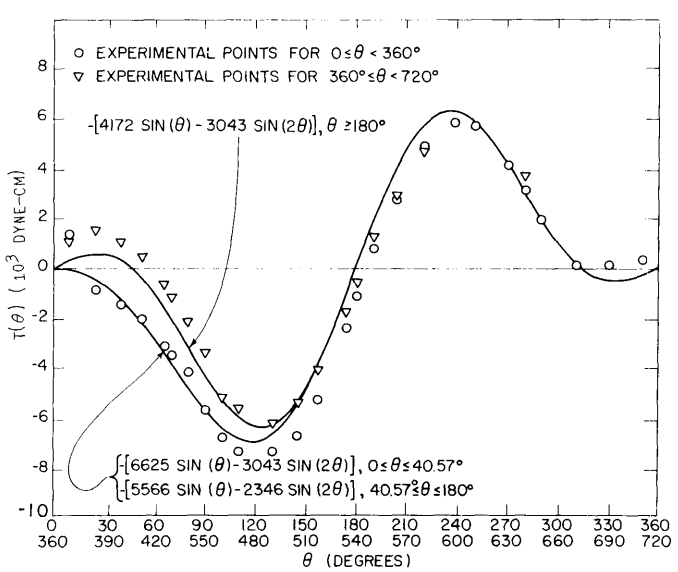

Fig. 14 - Torque for the split torus cooled with $B = 1000$ G and $\theta = 0$, and rotated with $B = 200$ G (magnetic transition)

SPLIT TOROID OF ELONGATED CROSS SECTION

Figure 15 shows the geometrical features of the split toroid of elongated cross section used in the experiments. Except for the thin cross-sectional slice which has been

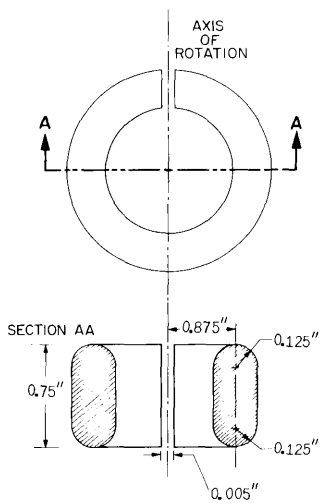

Fig. 15 - Geometry of the split toroid of elongated cross section

removed, this split toroid is identical in size and shape to the toroid of elongated cross section illustrated in Fig. 6 and is also fabricated of well-annealed lead having 0.9999 purity.

Figure 16 shows the experimental results when the split toroid of elongated cross section becomes superconducting with $B = 0$ and $\theta_i = 0$. Then B is raised to 100 G, and the split toroid is rotated through 2π radians while B is kept at 100 G.

Equation (10), with $B_2(\theta)$ identically zero and with $(\Delta X - \Delta K_c^{\parallel})$ negligible compared to $(K_m^{\perp} - K_m^{\parallel})$, is applicable in this case. In other words, the equation

$$T = -e_z(1/2)(K_m^{\perp} - K_m^{\parallel})B^2 \sin(2\theta)$$

should fit the data points fairly well. The application of least-square curve fitting yields a value of 4510 dyne-cm for $(1/2)(K_m^{\perp} - K_m^{\parallel})B^2$, from which it follows that $(K_m^{\perp} - K_m^{\parallel}) =$ 0.9020 dyne-cm/G^2. This value is reasonably close to 1.225 dyne-cm/G^2, the experimentally determined value of $(K_m^{\perp} - K_m^{\parallel})$ for the toroid of Fig. 6. The reason that the toroid of elongated cross section, described in Fig. 6, and the split toroid of elongated cross section, described in Fig. 15, have roughly the same $(K_m^{\perp} - K_m^{\parallel})$ is that both are the same size and shape, with the exception of the small cross-sectional slice which has been removed from the split toroid.

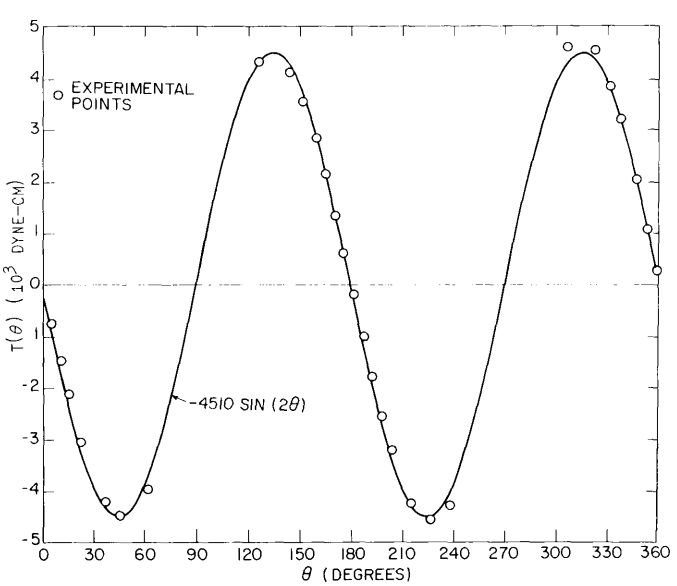

Fig. 16 - Torque for the split toroid of elongated cross section cooled with $B = 0$ and $\theta = 0$, and rotated with $B = 100$ G

A CASE WHERE $\theta_i \neq 0$

All the experiments discussed thus far have been arranged so that $\theta_i = 0$, largely because the interpretation of the experimental results in the light of the theoretical model is significantly more difficult when $\theta_i \neq 0$ than when $\theta_i = 0$. (If $\theta_i \neq 0$, then the $B_3(\theta)$ in Eq. (8) cannot be taken to be identically zero.) However, substantial simplification results if one restricts oneself to situations in which B is always kept small enough to insure that criticality never occurs. In such situations $B_2(\theta) = B_2(\theta_i) = B_i \cos(\theta_i)$, and $B_3(\theta) = B_3(\theta_i) = -B_i \sin(\theta_i)$ for all θ. If a split toroid is used, $B_1(\theta) = 0$ for all θ, and $K_c^{\parallel} = 0$. Then Eq. (8) becomes

$$T = -e_z\left[\Delta K_c^{\parallel} B B_i \cos(\theta_i)\sin(\theta) + \frac{1}{2}(K_m^{\perp} - K_m^{\parallel}) B^2 \sin(2\theta) + \Delta K_c^{\perp} B B_i \sin(\theta_i)\cos(\theta)\right] . \quad (12)$$

(As in the derivation of Eq. (9), the approximation $(\Delta K_m^{\perp} - \Delta K_m^{\parallel} - \Delta K_c^{\parallel} + \Delta K_c^{\perp}) \approx 0$ for small B has been used.)

Figure 17 shows the results of an experiment in which the split toroid of elongated cross section becomes superconducting with B_i = 100 G and $\theta_i = \pi/4$ and is then rotated through 4π radians with B = 100 G. Data points in the range $\pi/4 \leq \theta \leq 9\pi/4$ are shown. Figure 12 also shows the curve $T(\theta) = -[C_1 \sin(\theta) + C_2 \sin(2\theta) + C_3 \cos(\theta)]$, where C_1, C_2, and C_3 have been determined by the application of least-square methods to the experimental data points. One finds that C_1 = 581.0 dyne-cm, C_2 = 4304 dyne-cm, and C_3 = -6636 dyne-cm, from which it follows that $\Delta K_c^{\parallel}$ = 0.08216 dyne-cm/G^2, $\Delta K_c^{\perp}$ = -0.9384 dyne-cm/G^2, and $(K_m^{\perp} - K_m^{\parallel})$ = 0.8606 dyne-cm/G^2. This value of $(K_m^{\perp} - K_m^{\parallel})$ agrees reasonably well with 0.9020 dyne-cm/G^2, the value found from an analysis of the experimental data pertaining to Fig. 16.

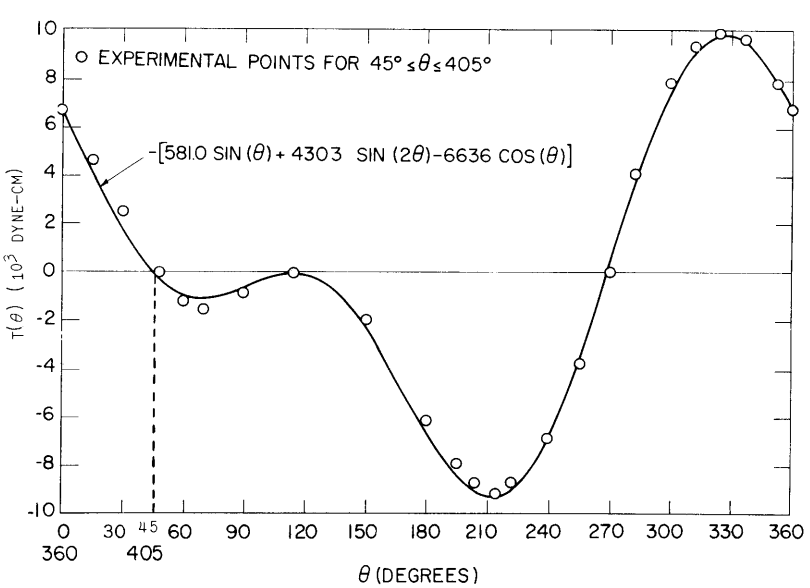

Fig. 17 - Torque for the split toroid of elongated cross section cooled with B = 100 G and θ = 45°, and rotated with B = 100 G

SUMMARY

The torque on a toroid arbitrarily oriented in a uniform field may be explained in terms of magnetic-moment components produced by persistent currents, and the Meissner effect. The essential feature of this determination has been the evaluation of the total moment as a function of moment components parallel to and perpendicular to the torus axis. The mathematical model describing the torque matches the measured results to within experimental error, if incipient critical fields on the torus surface are considered.

It is notable that, once having occurred, these fields result in a hysteresis whereby torques experienced at specified angles in the first 2π toroidal rotation differ in magnitude from those of the second rotation. In the first rotation the moment components due to persistent currents or trapped fields effectively adjust themselves at the onset of critical surface fields to maintain superconductivity or flux exclusion in the toroid. Once this adjustment is made on the first rotation, torque variations on the second and subsequent traversals are repetitive. It is significant that the determination of critical surface fields is much more tenuous for the more general toroidal configurations than for the torus, and this tenuity must be resolved if the analytical model is to be useful in the torque problem when criticality is encountered.

In applying the analytical model it was found that a critical field B_c of about 590 G allowed a closer matching of calculated torques with measured torques than did the expected value of 540 G. Specimen properties and conditioning are known to effect this B_c, upon which the torque calculations are dependent. Therefore, a determination of B_c for the particular material used is advisable in order to gain the best results from the model.

It was possible to treat the effects of trapped or pinned fields only qualitatively and to show their consistency with experimental behavior and their nature as a body-type inclusion. The relatively high purity (0.9999) lead used in these experiments exhibited significant trapping.

ACKNOWLEDGMENTS

The authors express their appreciation to the personnel of the Research Computation Center of the Naval Research Laboratory for their advice relating to the programming of the Laboratory's digital computer.

In addition, the authors express their appreciation to the following persons in the Energy Conversion Branch: Mr. P. I. Peterson, for his assistance in making measurements and in analyzing data during the initial phases of the experiments; Mr. E. B. Wright, for his advice concerning the approximation of the Meissner moment constants for a toroid of elliptical cross section; and Mr. W. K. Gardner for the curves appearing in Figs. 7, 13, 14, 16, and 17, which he constructed using an analog computer and x-y plotter.

REFERENCES

1. Wright, E.B. and Peterson, P.I., "Potential and Magnetic Moment of a Superconducting Torus in a Non-Axial Uniform Magnetic Field," NRL Report 6429, Oct. 18, 1966; also, "Magnetization of an Ideal Superconducting Torus in a Transverse Field," J. Appl. Phys. 38(2):855-860 (1967)

2. Shoenberg, D., "The Magnetization Curves of a Superconducting Sphere and Ring," Proc. Roy. Soc. (London) A155:712 (1936); also Shoenberg, D., "Superconductivity," 2nd ed., reprinted, London:Cambridge University Press, 1962

3. de Launay, J., "Electrodynamics of a Superconducting Torus," NRL Report P-3441, April 1949

4. King, E.E., "The Magnetic Torque of Ideal Superconducting Toroids," NRL Report 6414, August 1966

5. Wilson, B.J., and King, E.E., "Torque on a Superconducting Torus in a Uniform Field," J. Appl. Phys. 38(2):745-752 (1967)

6. Shoenberg, D., "The Magnetization Curves of a Superconducting Sphere and Ring," Proc. Roy. Soc. (London) A155:725 (1936)

7. Fritz, J.J., Gonzalez, O.D., and Johnston, H.L., "Magnetic Moments and Eddy Currents in Spheres of Superconducting Tin," Phys. Rev. 80:894 (1950)

8. Carroll, K.J., "Residual Magnetic Moments of Some Elementary Superconducting Spheres," Cryogenics 5:199 (1965)

This page intentionally left blank.

Security Classification

DOCUMENT CONTROL DATA - R & D

(Security classification of title, body of abstract and indexing annotation must be entered when the overall report is classified)

1. ORIGINATING ACTIVITY *(Corporate author)*

Naval Research Laboratory
Washington, D.C. 20390

2a. REPORT SECURITY CLASSIFICATION

Unclassified

2b. GROUP

3. REPORT TITLE

TORQUE ON A SUPERCONDUCTING TOROID IN A UNIFORM FIELD

4. DESCRIPTIVE NOTES *(Type of report and inclusive dates)*

A final report on one phase of the problem; work on other phases continues.

5. AUTHOR(S) *(First name, middle initial, last name)*

B.J. Wilson, E.E. King, and J.R. Miller

6. REPORT DATE

December 5, 1967

7a. TOTAL NO. OF PAGES

26

7b. NO. OF REFS

8

8a. CONTRACT OR GRANT NO.

NRL Problem E01-01

b. PROJECT NO.

RR 010-04-41-5950.101

c.

d.

9a. ORIGINATOR'S REPORT NUMBER(S)

NRL Report 6618

9b. OTHER REPORT NO(S) *(Any other numbers that may be assigned this report)*

10. DISTRIBUTION STATEMENT

This document has been approved for public release and sale; its distribution is unlimited.

11. SUPPLEMENTARY NOTES

12. SPONSORING MILITARY ACTIVITY

Department of the Navy (Office of Naval Research), Washington, D.C. 20360

13. ABSTRACT

The torques on superconducting lead toroids immersed in various uniform fields were measured and calculated as a function of angular position. The calculations, based on ideal superconducting behavior, agree with experiment for the closed torus, if persistent current decrease due to critical surface fields is considered. The recognition of trapped-flux phenomena is needed to explain the measured results for the open torus, when it has been cooled in a nonzero field or when a magnetic transition to superconductivity has been made. The analytical model used magnetic moments for a torus in an axial field and in a perpendicular field, rigorously calculated elsewhere. These methods of obtaining approximations to the moments presented may possibly apply to more general toroidal bodies. The total magnetic moment (and thus the torque) for arbitrary angular position is found by superposition, a result not previously obtained.

DD FORM 1 NOV 65 1473 (PAGE 1)

S/N 0101-807-6801

Security Classification

Security Classification

14. KEY WORDS	LINK A ROLE	LINK A WT	LINK B ROLE	LINK B WT	LINK C ROLE	LINK C WT
Magnetic moment						
Torque						
Toroid						
Superconductor						
Flux exclusion						
Criticality						
Trapped fields						

DD FORM 1 NOV 65 1473 (BACK) (PAGE 2)

GPO 934-240

Security Classification